

Antifreeze proteins and homogeneous nucleation: On the physical determinants impeding ice crystal growth ^{EP}

Cite as: J. Chem. Phys. **153**, 091102 (2020); <https://doi.org/10.1063/5.0023211>

Submitted: 27 July 2020 . Accepted: 19 August 2020 . Published Online: 04 September 2020

Valentino Bianco , Jorge R. Espinosa , and Carlos Vega 

COLLECTIONS

 This paper was selected as an Editor's Pick



View Online



Export Citation



CrossMark

Lock-in Amplifiers
up to 600 MHz



Watch



Antifreeze proteins and homogeneous nucleation: On the physical determinants impeding ice crystal growth

Cite as: J. Chem. Phys. 153, 091102 (2020); doi: 10.1063/5.0023211

Submitted: 27 July 2020 • Accepted: 19 August 2020 •

Published Online: 4 September 2020



View Online



Export Citation



CrossMark

Valentino Bianco,^{1,a)}  Jorge R. Espinosa,^{2,3}  and Carlos Vega^{1,a)} 

AFFILIATIONS

¹Faculty of Chemistry, Chemical Physics Department, Universidad Complutense de Madrid, Plaza de las Ciencias, Ciudad Universitaria, Madrid 28040, Spain

²Maxwell Centre, Cavendish Laboratory, Department of Physics, University of Cambridge, Cambridge CB3 0H3, United Kingdom

³Emmanuel College, Cambridge CB2 3AP, United Kingdom

^{a)}Authors to whom correspondence should be addressed: vbianco283@gmail.com and cvega@ucm.es

ABSTRACT

Antifreeze proteins (AFPs) are biopolymers capable of interfering with ice growth. Their antifreeze action is commonly understood considering that the AFPs, by pinning the ice surface, force the crystal–liquid interface to bend forming an ice meniscus, causing an increase in the surface free energy and resulting in a decrease in the freezing point ΔT^{\max} . Here, we present an extensive computational study for a model protein adsorbed on a TIP4P/Ice crystal, computing ΔT^{\max} as a function of the average distance d between AFPs, with simulations spanning over 1 μ s. First, we show that the lower the d , the larger the ΔT^{\max} . Then, we find that the water–ice–protein contact angle along the line $\Delta T^{\max}(d)$ is always larger than 0° , and we provide a theoretical interpretation. We compute the curvature radius of the stable solid–liquid interface at a given supercooling $\Delta T \leq \Delta T^{\max}$, connecting it with the critical ice nucleus at ΔT . Finally, we discuss the antifreeze capability of AFPs in terms of the protein–water and protein–ice interactions. Our findings establish a unified description of the AFPs in the contest of homogeneous ice nucleation, elucidating key aspects of the antifreeze mechanisms and paving the way for the design of novel ice-controlling materials.

Published under license by AIP Publishing. <https://doi.org/10.1063/5.0023211>

I. INTRODUCTION

Many living beings facing drastic environmental conditions have evolved in order to adapt to large temperature excursions, as observed in bacteria,¹ fungi,² plants,³ insects,⁴ and vertebrates,⁵ living in the depths of the oceans, perennial snows, or desert areas. Freezing regulation activity involves one of the most difficult recognition problems in biology, the distinction between ice and liquid water.^{6,7} The key point is the ability of a class of proteins, known as antifreeze proteins (AFPs),⁸ to control the liquid and solid phases of the most important substance for life: water.

According to a widely accepted adsorption–inhibition mechanism, proposed by Raymond and DeVries,^{9,10} the AFPs bind the ice surface, causing a local increase in the curvature. This depresses the

freezing point by $\Delta T^{\max} \equiv T_m - T_f$ according to the Gibbs–Thomson effect,^{11–13} where T_m is the thermodynamic melting temperature and T_f is the effective freezing temperature (see the [supplementary material](#)). This would suggest that AFPs avoid the growth of a post-critical ice nucleus rather than impeding the formation of an ice nucleus. Nevertheless, despite a growing body of the literature on ice-binding proteins,^{6–9,11,12,14–32} a complete study on the antifreeze effect of the AFP concentration on the ice growth is still missing.

The theory proposed in Ref. 9 assumes AFPs regularly arranged on a square lattice on top of the ice surface. This minimal model *square proteins on a square lattice* can be exploited in simulations to investigate the AFP mechanisms. Following such an approach, in this work, we present an extensive study for a model of AFPs immersed in TIP4P/Ice water³³—a model that

quantitatively accounts for many ice thermodynamic and structural properties^{34,35}—on the antifreeze capability of AFPs according to their expression level (proportional to the concentration of proteins absorbed onto ice). We establish the decrease in the freezing point, ΔT^{\max} , according to the protein–protein distance d by means of extensive molecular dynamic simulations. We show how the ice interface between two proteins bends forming a meniscus. We predict (for the first time as far as we know) the $\Delta T^{\max} - d$ curve for a simple square coarse-grained model of proteins, in simulations on the microsecond scale, showing that at the ice percolation point, the contact angle θ is larger than 0° . We also discuss an interpretation of our results, in connection with theories^{9,25} and experimental data.^{12,26} Finally, we characterize the ice growth according to the water–protein interaction and protein size.

II. METHODOLOGY

We consider an ice slab composed of several layers (>10), flanked by two AFPs [Figs. 1 and 1(a) of the [supplementary material](#)] irreversibly bound to the ice.^{36,37} The ice is oriented with the basal plane toward the binding protein³⁸ and filling completely the X and Y dimensions of the simulation box. The protein structure is coarse-grained respecting the average size⁸ and composition^{39,40} of the AFPs; more details are provided in the [supplementary material](#). Given a XYZ simulation box, the ice would expand along the Z direction (Fig. 1). The relevant linear dimension for the ice to grow is d , i.e., the available space between the AFP and its replica through the periodic boundary conditions along the diagonal of the XY plane [Fig. 1(a)]. By changing L_x and L_y —hence d —we mimic different concentrations of the AFP absorbed on ice.

We perform anisotropic NpT simulations, with $p = 1$ bar, for systems ranging from $N = 8131$ to $N = 120\,768$ water molecules, corresponding to $d \in [2.7: 16.2]$ nm, with temperatures spanning from $T = 250$ K to $T = 269$ K, below the melting point of the water model $T_m = 270$ K.³⁵ Each run extends up to ~ 1 μ s, which is a time window reasonably longer than the time required for the ice to grow.^{41,42} The number of ice molecules is determined according to the \bar{q}_6 order parameter,⁴³ with a cutoff of 3.5 Å and a threshold of $\bar{q}_6 > 0.37$.⁴⁴

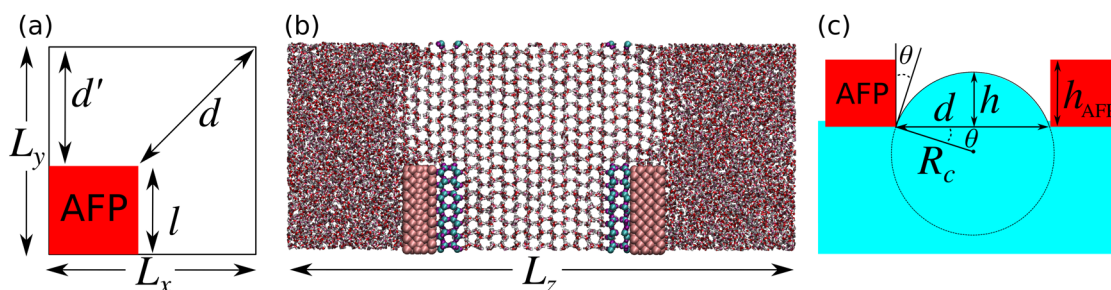


FIG. 1. (a) Back view of the *square protein* on a *square lattice* AFP model along the XY plane. The AFP is modeled with atoms arranged in a tangent fcc lattice, interacting with water via a Lennard-Jones potential with $\epsilon = 0.5$ kJ/mol and $\sigma = 0.316$ 68 nm. The maximum distance between two AFPs is $d \equiv [(L_x - l)^2 + (L_y - l)^2]^{1/2}$, where $L_x \sim L_y$ are the X and Y sizes of the box and $l \times l \times h_{\text{AFP}}$ are the AFP sizes. $l = 2.5$ nm and $h_{\text{AFP}} = 1.2$ nm (including the van der Waals radius) are comparable with linear sizes observed in AFPs.⁸ $d' = d/\sqrt{2}$. (b) Solid–liquid equilibrium interface for $N = 17\,584$ water molecules at $T = 264$ K, with $d \sim 5.4$ nm. (c) Scheme of the antifreeze mechanism (seen from the diagonal) proposed in Ref. 9. R_c is the curvature radius, and θ is the contact angle.

III. RESULTS

In Fig. 2, we report the fraction of ice molecules as a function of time, for two values of d (see also Fig. 2 of the [supplementary material](#)). For sufficiently high temperatures— $T \geq 264$ K and $T \geq 254$ K in the cases shown in Fig. 2—the presence of the AFPs impedes the ice growth. The ice surface distorts forming a meniscus, whose dome protrudes into the bulk supercooled water [Figs. 1(b) and 1(c)], consistent with that observed in other simulation studies with TIP4P water and⁴⁵ mW water²⁵ and in experiments.⁴⁶ The shape of the solid–liquid interface is stable within the explored time window of ~ 1 μ s, resembling a sphere along d and a cylinder along d' , as shown in Fig. 3, for $d \sim 5.4$ nm (see Fig. 7 of the [supplementary material](#) for $d \sim 4.1$ nm). By decreasing T , the solid–liquid interface further bends, increasing its curvature and expanding into the liquid phase. When the mechanical stability is passed, the ice overgrows the AFPs wrapping it [see Figs. 1(b)–1(d) of the [supplementary material](#)], as observed also in Ref. 25.

The lowest temperature T_f at which the AFPs impede the ice growth according to d defines the lowering of the freezing point $\Delta T^{\max} \equiv T_m - T_f$. We clearly observe that ΔT^{\max} increases by decreasing d , as shown by black points in Fig. 4. Our data are well fitted by $\Delta T^{\max} \propto d^{-4}$ (blue dashed line in Fig. 4). Interestingly, when $d \sim 7$ nm, we found $\Delta T^{\max} \sim 0.5$ K, close to the thermal hysteresis ~ 0.72 K experimentally observed in the Tenebrio molitor’s AFP separated by an analogous distance²⁶ (red square in Fig. 4). For $d \geq 7.8$ nm, the ice growth is inevitable [see Figs. 2(d) and 2(e) of the [supplementary material](#)].

Raymond and DeVries proposed a relation between the supercooling $\Delta T \equiv T_m - T \leq \Delta T^{\max}$ and the protein distance d , given by^{9,47}

$$\Delta T = \alpha_p \left(\frac{\gamma_{sl} T_m v}{\Delta H_m} \right) \frac{\cos \theta}{d}, \quad (1)$$

where α_p is a geometrical factor ($\alpha_p = 4$ and 2 for spherical and cylindrical interfaces, respectively), γ_{sl} is the solid–liquid surface free energy, v is the molar volume of ice, ΔH_m is the molar latent heat of melting, and θ is the contact angle [Fig. 1(c)]. When the system reaches a metastable equilibrium at ΔT , the chemical potentials of the liquid and solid phases [the solid being at higher pressure

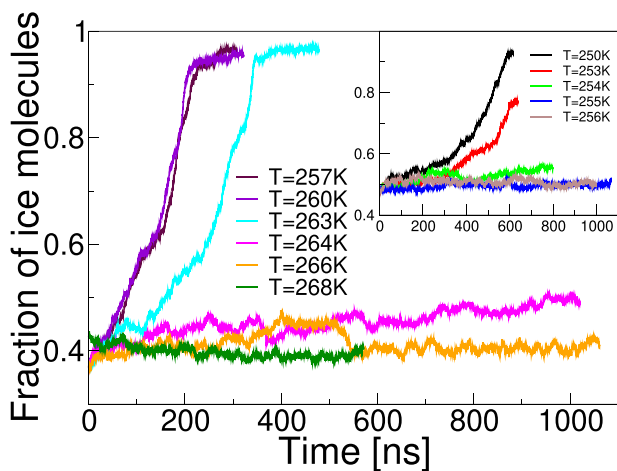


FIG. 2. Time evolution of the fraction of ice molecules, for different T . The number of water molecules is $N = 17\,584$, with $d \sim 5.4$ nm. The inset refers to $N = 13\,130$ water molecules, with AFPs separated by $d \sim 4.1$ nm.

due to the curved interface as described by the Laplace's equation $\Delta p = \alpha p \gamma_{sl} / (2R_c)$ are equal. By decreasing T , the angle θ decreases. Raymond and DeVries assumed that the stability limit of the interface is reached when $2R_c = d$ for the spherical interface ($2R_c = d'$ for the cylindrical one), corresponding to the minimum angle of $\theta^{\min} = 0$ [Fig. 1(c)]. As shown in Fig. 4, this assumption leads to ΔT^{\max} considerably larger than the outcome of our simulations (longer runs could increase the deviation by decreasing ΔT^{\max} for each value of d). This suggests that along the locus $\Delta T^{\max}(d)$, we have always $\theta^{\min}(\Delta T^{\max}) > 0$. Thus, the hypothesis of Raymond and DeVries that the ice spans only when $\theta \sim 0$ is not consistent with our results. Certainly, the interfacial free energy for the ice–water interface of the TIP4P/Ice model of water may differ from that of real water. However, in this work, we are comparing the results of the simulation obtained with TIP4P/Ice with the results of the theory for the same model so that the differences point out the limitations of the theory.

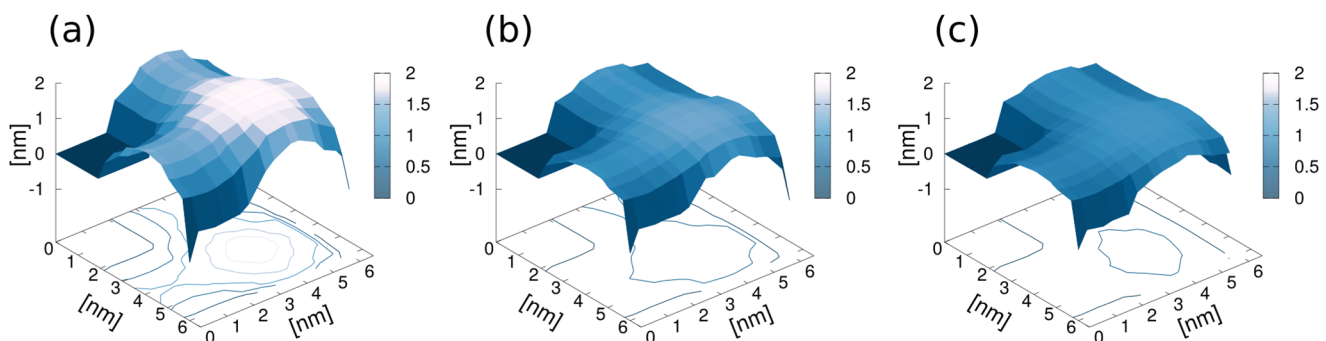


FIG. 3. Ice surface in a system with $N = 17\,584$ water molecules, $d \sim 5.4$ nm, for (a) $T = 264$ K, (b) $T = 266$ K, and (c) $T = 268$ K. The AFP anchors the ice in the darkest/square region corresponding to null height. On the XY plane are shown the level lines corresponding to the ice heights 0.5 nm, 1.1 nm, 1.45 nm, 1.75 nm, and 1.85 nm, from the darker to the clearer color, respectively.

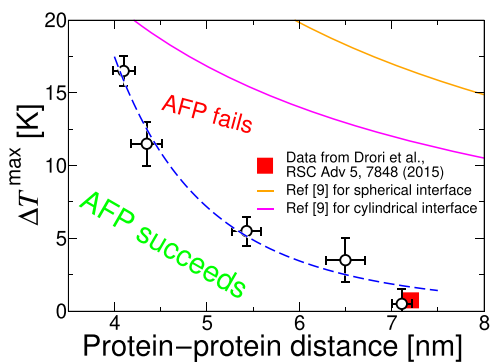


FIG. 4. Decrease in the freezing point ΔT^{\max} as a function of the average protein–protein distance d . The blue dashed line is a fit $\Delta T^{\max} = 4476.52/d^4$. Continuous lines are given by Eq. (1), with $\theta = \theta^{\min} = 0$, $\nu = 1.99 \times 10^{-5}$ m³/mol, $\Delta H_m = 5397$ J/mol (the melting enthalpy of the TIP4P/Ice model), and $\alpha p = 2, 4$ for a cylindrical or spherical interface, respectively. For any d , ΔT^{\max} for the cylindrical interface is computed for d' [Fig. 1(a)].

To verify this, we computed θ for $d \sim 4.1$ nm and $d \sim 5.4$ nm, for $\Delta T \leq \Delta T^{\max}$, reported in Fig. 5(a) (see the [supplementary material](#) for details). The full point marks θ^{\min} (and ΔT^{\max}): by further decreasing T , the solid–liquid interface is no longer stable, and the ice percolates through the system. The value of θ can be predicted following the work of Naullage, Qiu, and Molinero.²⁵ Indeed, the authors have successfully derived the expression for the θ -dependence of the Gibbs free energy difference ΔG for a cylindrical solid–liquid interface.²⁵ Accordingly, they show that, for $\Delta T < \Delta T^{\max}$, the predicted ΔG exhibits a local minimum for values of θ consistent with their findings. We extended such an approach for a spherical interface (see the [supplementary material](#)),

$$\Delta G = -\Delta\mu_{\text{ice}} \frac{\pi d^3}{24 \cos^3 \theta} (\sin^3 \theta - 3 \sin \theta + 2) + \frac{\gamma_{sl} \pi d^2}{2} \left[\frac{1 - \sin \theta}{\cos^2 \theta} - \frac{1}{2} \right] + \tau \ell, \quad (2)$$

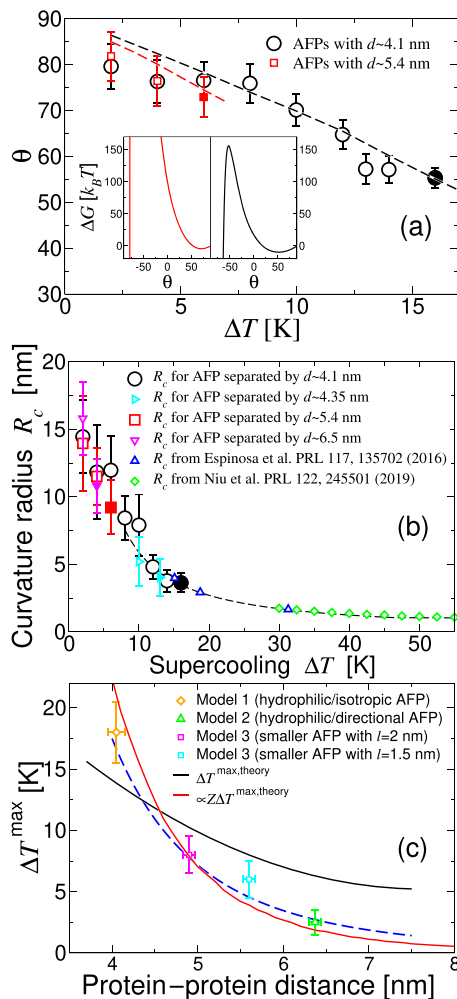


FIG. 5. (a) Contact angle θ of the spherical dome as a function of ΔT for two d . Full points mark θ^{\min} . Dashed lines are the predictions given by the minimum of ΔG in Eq. (2). Inset: ΔG given by Eq. (2) at the spanning points, $T = 253$ K for $d \sim 4.1$ nm (black curve), and $T = 263$ K for $d \sim 5.4$ nm (red curve). (b) R_c as a function of ΔT , for various d . Full points mark the maximum supercooling ΔT^{\max} (minimum R_c). The black dashed line is a power law fit of the data from Refs. 48 and 49. (c) Change in ΔT^{\max} according to the model variation. The blue dashed line is the fitting curve of Fig. 4. Continuous lines are the theoretical predictions described in the text.

where $\Delta\mu$ is the difference between the liquid and solid chemical potentials in bulk, ρ_{ice} is the ice's number density, τ is the line tension, and ℓ is the length of the AFP–solid–liquid contact line (following Ref. 25, we shall neglect the $\tau\ell$ term). The condition $\partial\Delta G/\partial\theta = 0$ together with the approximation $\Delta\mu = \Delta H_m\Delta T/T_m$ leads to Eq. (1). Figure 5(a) reveals that the theory correctly predicts the equilibrium contact angle for $\Delta T < \Delta T^{\max}$. In addition, for $\Delta T \sim 2$ K, the theory predicts $\theta \sim 86^\circ$, in reasonable agreement with $\theta = 88.0^\circ \pm 1.3^\circ$ observed by Karlsson *et al.*¹² for small supercooling (up to 2.4 K). Nevertheless, as we show in the inset of Fig. 5(a), Eq. (2) predicts stable solid–liquid interfaces with huge free energy barriers (in $k_B T$ unit) from the stable state $\theta = -90^\circ$ at the $\Delta T = d$ conditions where

we observed the ice spanning (Fig. 2). Hence, Eq. (2) allows an estimation of θ for each T but, as anticipated in Ref. 25, does not allow one to estimate ΔT^{\max} for a certain d . Contact angles in the cylindrical region of the interface (along d' in Fig. 1) are smaller than those of the spherical interface, as can be seen in Fig. 5 of the SM but are not zero at the conditions where we observed the ice spanning.

We focus now on ΔT dependence of the curvature radius R_c of the solid–liquid interface. From the spherical dome of the average stable ice surface shown in Fig. 3, we extract R_c and compare it with the T -dependence of the critical ice radii established from studies of homogeneous nucleation⁵⁰ for the same water model.^{48,49} The reasonable agreement shown in Fig. 5(b) confirms that the stable solid–liquid interfaces observed in simulations, and predicted by Eq. (2) following Ref. 25, have the curvature established by the Classical Nucleation Theory (CNT). Thus, according to CNT (and consistent with our findings), in the homogeneous and heterogeneous nucleation and AFP, the value of R_c is determined uniquely by ΔT (although θ is determined by the Young equation in heterogeneous nucleation and by d for AFPs).

The data $\Delta T^{\max}(d)$, as observed also in Ref. 25, can be explained considering that, in order to span, the height h of the ice meniscus must overcome the AFP's height h_{AFP} [Fig. 1(c)]. As shown in the supplementary material, by imposing that the stability limit of the solid–liquid interface is reached when the ice dome [whose height can be expressed in terms of $\Delta\mu(T)$, $\gamma_{sl}(T)$, and $\rho_{\text{ice}}(T)$] matches h_{AFP} , we predict a decrease in ΔT^{\max} with d that qualitatively captures our simulation results, as shown by the black curve in Fig. 5(c) labeled $\Delta T^{\max}_{\text{theory}}$. Hence, h_{AFP} can be seen as the effective barrier to be overcome by the ice in order to span. This estimation can be further improved phenomenologically considering that, according to the CNT, the nucleation rate is $\propto Z \exp(-\Delta G/k_B T)$, where the Zeldovich factor $Z = \sqrt{\Delta\mu^4 \rho_{\text{ice}}^2 / (64\pi^2 k_B T \gamma_{sl}^3)}$ accounts for the curvature of the free energy curve at the top, and its inverse is related to the width of the region around the top.⁵¹

By rescaling the supercooling as $\Delta T^{\max}_{\text{theory},Z} \equiv AZ\Delta T^{\max}_{\text{theory}}$ (using $A \sim 1500$ as a fitting parameter), we get better agreement [red line in Fig. 5(c)]. Note that $\Delta T^{\max}(d)$ does not depend on the ice plane bound to the AFP (as long as the bond is stable) as γ_{sl} depends on R_c (the solid–liquid interface is curved) rather than on the plane from which the interface is lifted up.

Finally, we tested our findings against model variations. We considered the effect of a hydrophilic AFP interface facing the supercooled liquid water (i.e., all the protein sides not anchoring the ice). Hydrophilicity has been modeled by (i) increasing the depth of the isotropic water–protein potential to $\epsilon = 1$ kJ/mol (model 1) and (ii) freezing some disordered water molecules on the AFP surfaces exposed to the liquid and assuming these molecules to form part of the AFP structure, to allow the formation of directional water–AFP HBs (model 2). In both cases, ΔT^{\max} is consistent with what was previously found [Fig. 5(b)], suggesting that hydrophobicity of the AFP surface non-anchoring the ice does not play a relevant role in preventing the ice growth. Nevertheless, our results indicate that it could affect the time required for the ice to envelop the AFP (as discussed in the supplementary material). We also tested how the antifreeze activity depends on the protein size by computing ΔT for proteins with linear sizes $l = 2$ nm and $l = 1.5$ nm (keeping the value of h_{AFP} constant). Points labeled “model 3” in Fig. 5(b) reveal that l

does not affect the antifreeze capability. This occurs because of the perfect match between the surface of the AFP and the crystal structure, leading to a stable/irreversible AFP-ice binding. In this paper, we have not studied the impact of h_{AFP} on ΔT^{max} . However, our approximate theory [Fig. 5(b)] predicts an increase in ΔT^{max} with h_{AFP} as anticipated by Naullage *et al.*²⁵ For the square protein of this work, we did not find an important impact of l on ΔT^{max} in contrast to the result of Ref. 25. Further work to understand these subtle issues is needed.

IV. CONCLUSIONS

In this work, we present a broad computationally study on the capability of antifreeze proteins (AFPs) to prevent ice growth depending on their distance d along the ice surface and the supercooling ΔT .

The reader may wonder why we use d (and not d') to describe the value of ΔT^{max} . For a two-dimensional square lattice, the distance to the nearest neighbor d defines the lattice. However, it is observed in this work that the irreversible growth of ice occurs in the center of the square lattice and not along the sides of the square. Thus, in our view, it seems more useful to consider the direction from the AFP center to the point of the two-dimensional Wigner-Seitz cell, which is farthest away. For a simple square lattice, this direction is that of the diagonal of the square, and for this reason, d (rather than d') seems to be an appropriate parameter to describe the capacity of the AFP to avoid the formation of ice. In fact, this criterion could also be useful when considering non-regular arrangements of AFP in future work (by considering the Voronoi cells in this case).

By means of a minimal and controllable *square protein on a square lattice* model immersed at the solid-liquid interface of TIP4P/Ice water, we establish the lowering of the freezing point in a range $d \in [\sim 4: \sim 7]$ nm with simulations longer than a microsecond and characterize the curvature radius $R_c(T)$ and contact angle $\theta(T)$ of the solid-liquid interface. Our results indicate that along the $\Delta T^{\text{max}}(d)$ locus marking the stability limit of the solid-liquid interface—numerically captured by $\Delta T^{\text{max}} \sim d^{-4}$ —we have $\theta > 0$ (i.e., the ice meniscus is always smaller than a hemisphere): the Raymond and DeVries expression of Eq. (1)⁹ (with $\theta = 0$) cannot reproduce our simulation data for $\Delta T^{\text{max}}(d)$. Hence, analyzing previous theoretical approaches,^{9,25} we propose an interpretation for our findings. Moreover, we prove that $R_c(T)$ is consistent with the critical ice radius at the supercooled $T^{48,49}$ found in homogeneous nucleation. Finally, we studied how the antifreeze effect depends on the hydrophobicity and size of the AFP, revealing that, as long as the ice-AFP binding is stable, both the protein-ice contact area and the hydrophilic/hydrophobic AFP interface exposed to the liquid do not affect $\Delta T^{\text{max}}(d)$. Our analysis connects the physics of AFPs and the ice homogeneous nucleation into a unified picture, providing a step forward in understanding the chemical physics of AFPs, with findings possibly useful to design artificial ice-controlling materials.^{52–55} This work can be regarded as a first step. The model proposed here is simple as it reduces the chemical details of the AFPs by the irreversible bonding of an ice-blocking object bringing the problem closer to a physical description. Certainly, further work is needed to clarify the role of all the factors (water and protein models, height of the protein, shape of the two-dimensional lattice, etc.), and we

hope that this work stimulates further research on this interesting problem.

SUPPLEMENTARY MATERIAL

See the [supplementary material](#) for a description of the model used in this work, additional figures, and a complete description of the theory.

ACKNOWLEDGMENTS

The authors thank E. Sanz for helpful discussions and comments. V.B. acknowledges the support from the European Commission through the Marie Skłodowska-Curie Fellowship No. 748170 ProFrost. J.R.E. acknowledges funding from the Oppenheimer Research Fellowship and the Emmanuel College Roger Ekins Research Fellowship. This work was funded by Grant Nos. FIS2016-78117-P and PID2019-105898GB-C21 of the MEC and by Project No. UCM-GR17-910570 from UCM. The authors acknowledge the computer resources and technical assistance provided by the RES under Project No. QSB-2020-1-0010.

DATA AVAILABILITY

The data that support the findings of this study are available within the article and its [supplementary material](#).

REFERENCES

- 1 J. H. Lee, A. K. Park, H. Do, K. S. Park, S. H. Moh, Y. M. Chi, and H. J. Kim, *J. Biol. Chem.* **287**, 11460 (2012).
- 2 H. Kondo, Y. Hanada, H. Sugimoto, T. Hoshino, C. P. Garnham, P. L. Davies, and S. Tsuda, *Proc. Natl. Acad. Sci. U. S. A.*, **109**, 9360 (2012).
- 3 C. Sidebottom, S. Buckley, P. Pudney, S. Twigg, C. Jarman, C. Holt, J. Telford, A. McArthur, D. Worrall, R. Hubbard, and P. Lillford, *Nature* **406**, 256 (2000).
- 4 S. P. Graether, M. J. Kuiper, S. M. Gagné, V. K. Walker, Z. Jia, B. D. Sykes, and P. L. Davies, *Nature* **406**, 325 (2000).
- 5 C. B. Marshall, G. L. Fletcher, and P. L. Davies, *Nature* **429**, 153 (2004).
- 6 J. D. Madura, K. Baran, and A. Wierzbicki, *J. Mol. Recognit.* **13**, 101 (2000).
- 7 K. A. Sharp, *Proc. Natl. Acad. Sci. U. S. A.* **108**, 7281 (2011).
- 8 M. Bar Dolev, I. Braslavsky, and P. L. Davies, *Annu. Rev. Biochem.* **85**, 515 (2016).
- 9 J. A. Raymond and A. L. DeVries, *Proc. Natl. Acad. Sci. U. S. A.* **74**, 2589 (1977).
- 10 C. A. Knight, C. C. Cheng, and A. L. DeVries, *Biophys. J.* **59**, 409 (1991).
- 11 D. J. Kozuch, F. H. Stillinger, and P. G. Debenedetti, *Proc. Natl. Acad. Sci. U. S. A.* **115**, 13252 (2018).
- 12 J. O. M. Karlsson, I. Braslavsky, and J. A. W. Elliott, *Langmuir* **35**, 7383 (2019).
- 13 R. G. Pereyra, I. Szleifer, and M. A. Carignano, *J. Chem. Phys.* **135**, 034508 (2011).
- 14 D. R. Nutt and J. C. Smith, *J. Am. Chem. Soc.* **130**, 13066 (2008).
- 15 N. Smolin and V. Daggett, *J. Phys. Chem. B* **112**, 6193 (2008).
- 16 A. B. Siemer, K.-Y. Huang, and A. E. McDermott, *Proc. Natl. Acad. Sci. U. S. A.* **107**, 17580 (2010).
- 17 H. Nada and Y. Furukawa, *J. Phys. Chem. B* **112**, 7111 (2008).
- 18 H. Nada and Y. Furukawa, *Polym. J.* **44**, 690 (2012).
- 19 K. Meister, S. Strazdaite, A. L. DeVries, S. Lotze, L. L. C. Olijve, I. K. Voets, and H. J. Bakker, *Proc. Natl. Acad. Sci. U. S. A.* **111**, 17732 (2014).
- 20 K. Meister, S. Ebbinghaus, Y. Xu, J. G. Duman, A. DeVries, M. Gruebele, D. M. Leitner, and M. Havenith, *Proc. Natl. Acad. Sci. U. S. A.* **110**, 1617 (2013).
- 21 E. Duboué-Dijon and D. Laage, *J. Chem. Phys.* **141**, 22D529 (2014).
- 22 B. Kutschan, K. Morawetz, and S. Thoms, *Phys. Rev. E* **90**, 022711 (2014).

- ²³K. Meister, A. L. DeVries, H. J. Bakker, and R. Drori, *J. Am. Chem. Soc.* **140**, 9365 (2018).
- ²⁴Z. F. Brotzakis, I. K. Voets, H. J. Bakker, and P. G. Bolhuis, *Phys. Chem. Chem. Phys.* **20**, 6996 (2018).
- ²⁵P. M. Naullage, Y. Qiu, and V. Molinero, *J. Phys. Chem. Lett.* **9**, 1712 (2018).
- ²⁶R. Drori, P. L. Davies, and I. Braslavsky, *RSC Adv.* **5**, 7848 (2015).
- ²⁷J. Cheng, Y. Hanada, A. Miura, S. Tsuda, and H. Kondo, *Biochem. J.* **473**, 4011 (2016).
- ²⁸L. M. C. Olijve, K. Meister, A. L. DeVries, J. G. Duman, S. Guo, H. J. Bakker, and I. K. Voets, *Proc. Natl. Acad. Sci. U. S. A.* **113**, 3740 (2016).
- ²⁹H. Kim, J. Lee, Y. Hur, C. Lee, S.-H. Park, and B.-W. Koo, *Mar. Drugs* **15**, 27 (2017).
- ³⁰A. Kuffel, D. Czapiewski, and J. Zielkiewicz, *J. Chem. Phys.* **141**, 055103 (2014).
- ³¹J. Grabowska, A. Kuffel, and J. Zielkiewicz, *J. Chem. Phys.* **145**, 075101 (2016).
- ³²A. Kuffel, D. Czapiewski, and J. Zielkiewicz, *J. Chem. Phys.* **143**, 135102 (2015).
- ³³J. L. F. Abascal, E. Sanz, R. García Fernández, and C. Vega, *J. Chem. Phys.* **122**, 234511 (2005).
- ³⁴E. Sanz, C. Vega, J. R. Espinosa, R. Caballero-Bernal, J. L. F. Abascal, and C. Valeriani, *J. Am. Chem. Soc.* **135**, 15008 (2013).
- ³⁵M. M. Conde, M. Rovere, and P. Gallo, *J. Chem. Phys.* **147**, 244506 (2017).
- ³⁶Y. Celik, R. Drori, N. Pertaya-Braun, A. Altan, T. Barton, M. Bar-Dolev, A. Groisman, P. L. Davies, and I. Braslavsky, *Proc. Natl. Acad. Sci. U. S. A.* **110**, 1309 (2013).
- ³⁷N. Pertaya, C. B. Marshall, C. L. DiPrinzio, L. Wilen, E. S. Thomson, J. S. Wettlaufer, P. L. Davies, and I. Braslavsky, *Biophys. J.* **92**, 3663 (2007).
- ³⁸N. Pertaya, C. B. Marshall, Y. Celik, P. L. Davies, and I. Braslavsky, *Biophys. J.* **95**, 333 (2008).
- ³⁹V. Bianco, G. Franzese, C. Dellago, and I. Coluzza, *Phys. Rev. X* **7**, 021047 (2017).
- ⁴⁰S. Fukuchi and K. Nishikawa, *J. Mol. Biol.* **309**, 835 (2001).
- ⁴¹J. R. Espinosa, C. Navarro, E. Sanz, C. Valeriani, and C. Vega, *J. Chem. Phys.* **145**, 211922 (2016).
- ⁴²P. Montero de Hijes, J. R. Espinosa, C. Vega, and E. Sanz, *J. Chem. Phys.* **151**, 044509 (2019).
- ⁴³W. Lechner and C. Dellago, *J. Chem. Phys.* **129**, 114707 (2008).
- ⁴⁴J. R. Espinosa, C. Vega, C. Valeriani, and E. Sanz, *J. Chem. Phys.* **144**, 034501 (2016).
- ⁴⁵M. J. Kuiper, C. J. Morton, S. E. Abraham, and A. Gray-Weale, *eLife* **4**, e05142 (2015).
- ⁴⁶S.-S. Lu, T. Inada, A. Yabe, X. Zhang, and S. Grandm, *Int. J. Refrig.* **25**, 562 (2002).
- ⁴⁷E. Kristiansen and K. E. Zachariassen, *Cryobiology* **51**, 262 (2005).
- ⁴⁸J. R. Espinosa, A. Zaragoza, P. Rosales-Pelaez, C. Navarro, C. Valeriani, C. Vega, and E. Sanz, *Phys. Rev. Lett.* **117**, 135702 (2016).
- ⁴⁹H. Niu, Y. I. Yang, and M. Parrinello, *Phys. Rev. Lett.* **122**, 245501 (2019).
- ⁵⁰G. C. Sosso, J. Chen, S. J. Cox, M. Fitzner, P. Pedevilla, A. Zen, and A. Michaelides, *Chem. Rev.* **116**, 7078 (2016).
- ⁵¹K. F. Kelton and A. L. Greer, *Nucleation in Condensed Matter* (Pergamon, Elsevier, Oxford, 2010).
- ⁵²M. I. Gibson, *Polym. Chem.* **1**, 1141 (2010).
- ⁵³C. Cardelli, V. Bianco, L. Rovigatti, F. Nerattini, L. Tubiana, C. Dellago, and I. Coluzza, *Sci. Rep.* **7**, 4986 (2017).
- ⁵⁴C. Cardelli, F. Nerattini, L. Tubiana, V. Bianco, C. Dellago, F. Sciortino, and I. Coluzza, *Adv. Theory Simul.* **2**, 1900031 (2019).
- ⁵⁵J. Lee, S. Y. Lee, D.-K. Lim, D. J. Ahn, and S. Lee, *J. Am. Chem. Soc.* **141**, 18682 (2019).